EUROfusion Integrated Modelling (EU-IM) Capabilities and Selected Physics Applications

G.L. Falchetto[1], M.I. Airila[42], A. Alberto Morillas[29], E. Andersson Sundén[10], T. Aniel[1], J.-F. Artaud[1], O. Asunta[2,37], C.V. Atanasiu[36], M. Baelmans[27], V. Basiuk[1], R. Bilato[32], M. Blommaert[27], D. Borodin[16], C. Boulbe[28], S. Briguglio[11], J. Citrin[15], R. Coelho[25], S. Conroy[10], D. Coster[32], V. Doriæ[14], R. Dumont[1], E. Fable[32], B. Faugeras[28], J. Ferreira[25], L. Figini[19], A. Figueiredo[25], G. Fogaccia[11], C. Fuchs[32], E. Giovannozzi[11], V. Goloborod'ko[40], O. Hoenen[32], Ph. Huynh[1], F. Imbeaux[1], I. Ivanova-Stanik[23], T. Johnson[17], D. Kalupin[13], L. Kos[41], E. Lerche[30], J. Madsen[34], O. Maj[32], G. Manduchi[6], M. Mantsinen[18,29], Y. Marandet[33], S. Matejcik[8], R. Mayo-Garcia[29], P.J. McCarthy[38], A. Merle[12], E. Nardon[1], A.H. Nielsen[34], S. Nowak[19], M. O'Mullane[9], M. Owsiak[35], V. Pais[36], B. Palak[35], G. Pelka[23], M. Plociennik[35], G.I. Pokol[22], D. Poljak[14], H. Radhakrishnan[39], H. Reimerdes[12], D. Reiser[16], J. Romazanov[16], P. Rodrigues[25], X. Saez[3], D. Samaddar[4], O. Sauter[12], K. Schmid[32], B.D. Scott[32], S. Šesnić[14], J. Signoret[1], S.K. Sipilä[2], R. Stankiewicz[23], P. Strand[7], E. Suchkov[8], A. Šušnjara[14], G. Szepesi[4], D. Tegnered[7], K. Tőkési[20], D. Tskhakaya[40], J. Urban[24], P. Vallejos[17], D. Van Eester[30], L. Villard[12], F. Villone[5], B. Viola[11], G. Vlad[11], E. Westerhof[15], D. Yadykin[7], R. Zagorski[23], F. Zaitsev[8], T. Zok[35], W. Zwingmann[25], S. Äkäslompolo[2], the ASDEX Upgrade Team and the EUROfusion-IM Team[*]

E-mail contact of main author: *gloria.falchetto@cea.fr*

1 CEA, IRFM, F-13108 Saint Paul Lez Durance, France,
2 Aalto University, FIN-00076 Aalto, Finland,
3 Barcelona Supercomputing Center (BSC), Spain,
4 CCFE, Culham Science Centre, Abingdon, UK,
5 Consorzio CREATE, Cassino (FR), Italy,
6 Consorzio RFX, corso Stati Uniti 4, 35127 Padova, Italy
7 Department of Earth and Space Sciences, Chalmers University of Technology, Gothenburg, Sweden,
8 Department of Experimental Physics, Faculty of Mathematics, Physics and Informatics Comenius University Bratislava, Slovak Republic,
9 Department of Physics and Applied Physics, University of Strathclyde, Glasgow, UK,
10 Department of Physics and Astronomy, Uppsala University, SE-75120 Uppsala, Sweden,
11 ENEA, Dipartimento FSN, C. R. Frascati, Italy,
12 EPFL, Swiss Plasma Center , Lausanne, Switzerland,,
13 EUROfusion Programme Management Unit, Garching, Germany,
14 FESB - University of Split, 22000 Split, Croatia,
15 FOM Institute DIFFER, Eindhoven, The Netherlands,
16 Forschungszentrum Jülich GmbH, Jülich, Germany,
17Fusion Plasma Physics, EES, KTH, Stockholm, SE-10044 Sweden,
18ICREA-Barcelona Supercomputing Center (BSC), Barcelona, Spain
19 IFP-CNR, via R. Cozzi 53, 20125 Milano, Italy,
20 Institute for Nuclear Research, Hungarian Academy of Sciences, H-4026 Debrecen, Hungary
22 Institute of Nuclear Techniques, Budapest University of Technology and Economics, Budapest, Hungary
23 Institute of Plasma Physics and Laser Microfusion, Hery 23, 01-497 Warsaw, Poland
24 Institute of Plasma Physics CAS, Za Slovankou 1782/3, 182 00 Prague 8, Czech Republic
25 Instituto de Plasmas e Fusão Nuclear, Instituto Superior Técnico, Universidade de Lisboa, Portugal,
27 KU Leuven, Department of Mechanical Engineering, 3001 Heverlee, Belgium,
28 Laboratoire J.A.Dieudonné, F-06108 Nice CEDEX02, France,
29 Laboratorio Nacional de Fusión, CIEMAT, Madrid, Spain,
30 LPP-KMS ERM, B-1000 Brussels, Belgium,
32 Max-Planck-Institut für Plasmaphysik, D-85748 Garching, Germany,
33 PIIM, CNRS/Aix-Marseille Université, F-13397 Cedex 20, France,
34 PPFE, Department of Physics, Technical University of Denmark, Kgs. Lyngby, Denmark
35 Poznan Supercomputing and Networking Center, BCh PAS, Noskowskiego 12/14 Poznań, Poland
36 The National Institute for Laser, Plasma and Radiation Physics, Magurele-Bucharest, Romania,
37 Tokamak Energy Ltd, UK
38 University College Cork (UCC), Ireland,
39 University of Cyprus , Nicosia, Cyprus,
40 Fusion@ÖAW, Institute of Applied Physics, TU Wien, 1040 Vienna, Austria,
41 University of Ljubljana, Mech.Eng., Aškerčeva 6, 1000 Ljubljana, Slovenia,
42 VTT Technical Research Centre of Finland Ltd, P.O.Box 1000, FIN-02044 VTT, Finland

[*] http://www.euro-fusionscipub.org/eu-im

Abstract. Recent developments and achievements of the EUROfusion Code Development for Integrated Modelling project (WPCD), which aim is to provide a validated integrated modelling suite for the simulation and prediction of complete plasma discharges in any tokamak, are presented. WPCD develops generic complex integrated simulations, *workflows*, for physics applications, using the standardized European Integrated Modelling (EU-IM) framework. Selected physics applications of EU-IM workflows are illustrated in this paper.

1. Introduction

An extensive effort has been undertaken in Europe on the development of a standardized framework for self-consistent integrated modelling of tokamak plasmas, formerly under EFDA ITM-TF [1], pursued at present by the EUROfusion Code Development for Integrated Modelling project (WPCD). WPCD is developing generic and flexible sophisticated *workflows* for physics applications, aiming at providing a validated modular suite for the simulation of complete plasma discharges of any existing and future tokamak, including JT-60SA, ITER and DEMO. The EU-IM framework [2], which served as a basis for the development of ITER Integrated Modelling and Analysis Suite (IMAS [3]), is built around the backbone of a standardized data model, for the data exchange between the workflow components. The integration of physics codes in EU-IM workflows has besides been accompanied by a thorough cross-verification effort [4,5,6,7] which allows to trustfully choose the more appropriate model according to the required physics accuracy and computational time. The recent introduction of rigorous release procedures, for all workflow components, ensures quality and reproducibility of the simulations. Applications of EU-IM workflows to both interpretive and predictive studies are presented.

2. Predictive modelling with the European Transport Simulator, ETS

Among the main achievements, the European Transport Simulator (ETS) [8] has reached a capability equivalent to the state-of-the-art integrated modeling transport codes. The ETS, designed as a machine agnostic, modular and extensible workflow, offers a leading tool for transport analysis of any tokamak. It evolves the transport equations for plasma current, electrons and an arbitrary number of ion species including impurities in all ionization states, embedding interchangeable physics modules with different sophistication for magnetic equilibrium (both fixed and free boundary [1]), transport (interpretative, analytical, neoclassical, anomalous), neoclassical tearing modes (NTM), sawteeth, pellets including control, neutrals, Heating and Current Drive (HCD) sources for all the heating schemes (EC, NBI, IC, nuclear) including synergy effects among the latter (as demonstrated in [9]). Recently, the fixed-boundary core ETS has been released and deployed at JET, for application to interpretive analysis of experimental campaigns. Further, it is in use for predictive modelling of complex scenarios [10,11].

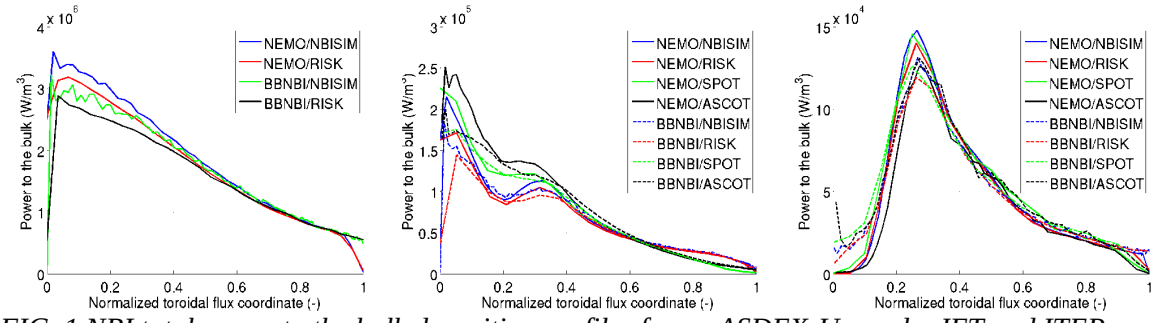

FIG. 1 NBI total power to the bulk deposition profiles for an ASDEX-Upgrade, JET and ITER case (left, center, right) for the 8 possible combinations of NBI codes. A good overall agreement is found. Wide orbits in ASCOT and SPOT codes cause losses at the edge and a reshaping of central profiles.

Specifically, flexible and sophisticated NBI modelling, for arbitrary injection geometries can be carried out, as part of an integrated ETS transport simulation. Beforehand, thorough cross-verification of all the possible combinations of the deposition codes (BBNBI [12], NEMO [13]) and the Fokker-Planck solvers (ASCOT [14], NBISIM [15], RISK [16], SPOT [17]) implemented in the ETS, was performed within the HCD workflow -run as standalone- for typical ASDEX-Upgrade and JET plasmas, as well as an ITER baseline scenario case [6]. The comparisons (FIG. 1) show good overall agreement among the coupled codes on the power to the bulk deposition and neutral beam current drive. Discrepancies arise when finite ion orbit width effects are not included in the Fokker-Planck calculations, as in the fast NBISIM and RISK codes, operating in the zero-banana-width limit.

An investigation of the effect of horizontal and vertical tilting of the neutral beam on the current drive (NBCD) and plasma heating in DEMO scenarios (prior to the baseline *EU DEMO1 2015* [18]) was then performed [11] using BBNBI and ASCOT within the ETS, for the case of peaked or flat density profile (FIG. 2). The simulations show that the shape of the driven current density profile strongly depends on the beam aiming and energy (FIG. 3).

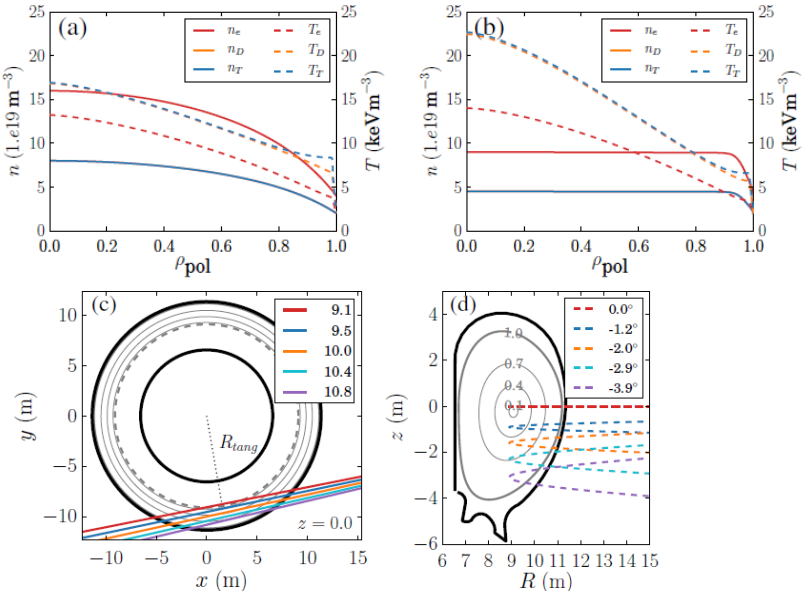

FIG. 2 Prescribed temperature and density profiles for the peaked (a) and flat (b) density scenario (both with n_D=n_T, I_p=16MA, B=6.79T). Magnetic equilibrium (d) calculated by CHEASE [18] within the ETS. NBI beamlines geometry (c,d). A model of ITER NBI injector was scaled up to DEMO dimensions. The reference case is horizontal injection (red line R_{tang}=9.1m, θ= 0.0°). Tilting the beams, the beamlines were aimed so that corresponding horizontally and vertically tilted beams had their tangency point at about the same ρ_{pol}.

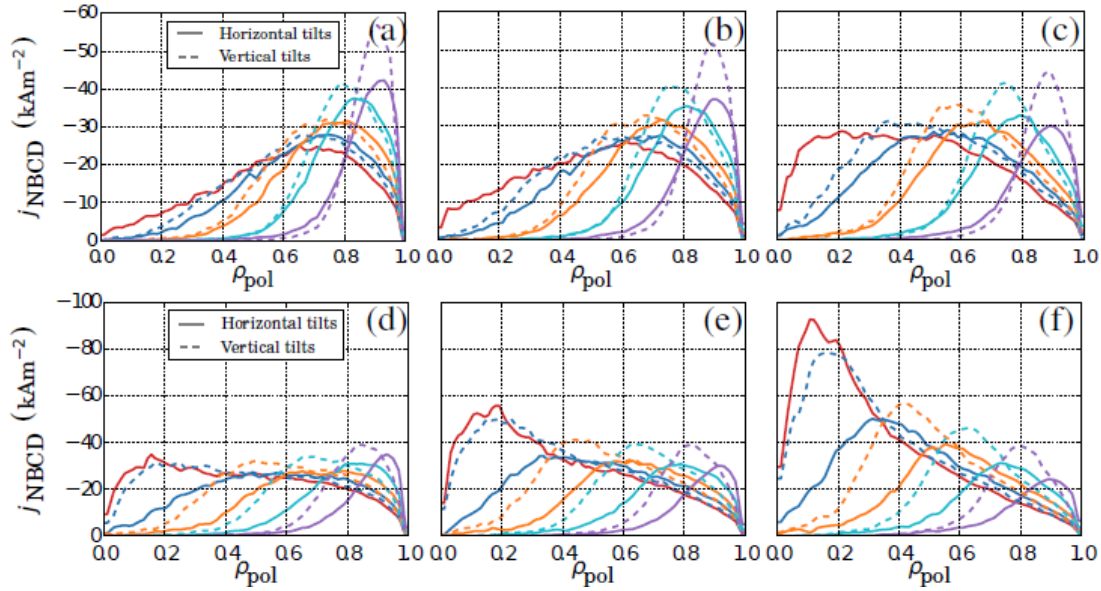

FIG. 3 NBCD current density for vertical (solid) and horizontal (dashed) tilted beams (colors as in FIG. 2 c-d) for the peaked (top plots) and flat (bottom plots) density scenario and beam energy of [0.75, 1.0, 1.5] MeV (left, center, right).

Low energy beams barely reach the plasma core, whereas tilting the beam horizontally or vertically moves the profile further outwards. The current drive appears to be a few per cent higher when tilting the beam vertically, compared to horizontal tilts.

Applications of the ETS also tackled plasma density control, as illustrated here for the case of a reactor-scale plasma fueled with multiple pellets [20]. A pellet module (derived from [21,22]) is implemented in the ETS providing the flux surface averaged changes to density and temperature profiles, treated by the transport solver as an instantaneous event. A newly developed algorithm for fueling control has been implemented in the ETS, offering two operational modes: specific injection times or fixed injection frequency. It provides density control on either volume averaged, line averaged (at given line) or local density (at given location). For the present study, the ETS was set up for evolving the transport equations for a reactor like plasma: $j_{//}$, T_e, T_i[D,T,He], n_i[D,T,He], including impurities with all charge states n_{imp}[Ar(1+:18+),W(1+:74+)], $T_{Ar}=T_W=T_D$. Transport coefficients were provided by a combination of Bohm-gyroBohm and neoclassical models (NEOS), assuming the edge transport barrier at $\rho_{tor\_norm}=0.97$. Heat and current drive sources were calculated by the NBI package, as above, and alpha heating module (*nuclearsim* [23]). Heat balance also included the radiation from impurities and synchrotron. The pellet controller was set to maintain the volume averaged density. Simulations were performed for five different injection locations, each with several pellet sizes and velocities.

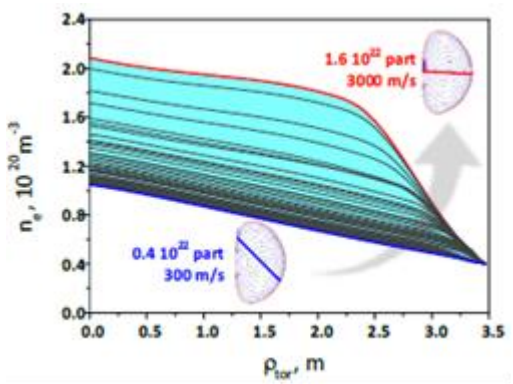

FIG. 4 Pellet cycle average electron density profiles from the ETS simulation for different pellet injection location, mass and velocity.

The injection frequency was adjusted inversely proportional to the pellet size so to keep the particle throughput constant over the scan.

As expected, the fueling efficiency increases with increasing velocity and size of injected pellets (FIG. 4). The flexibility of the pellet injector design in terms of injection angle was then addressed for the case of an intermediate size pellet ($6x10^{21}$ particles) with velocity of 1000 m/s. Results show that the density required for the foreseen reactor operational scenario can be maintained by a medium size pellet injected from the high field side. Besides, some flexibility in the pellet speed and injection angle is shown to be possible, keeping the same fueling efficiency.

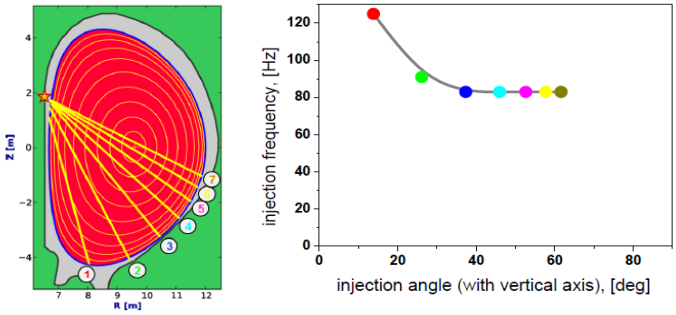

FIG. 5 Left: pellet injection angles, varied between 10°-70° (versus vertical axis), for a same entry point at the vessel. Right: pellet injection frequency adjusted by the controller as a function of injection angle. For trajectories 1-2 the deposition shifts outwards, fueling is less efficient, forcing the controller to increase the injection frequency in order to maintain the required density.

3. Edge - core coupling

Recently, edge-core coupling has been realized in the ETS by implementing in the Kepler workflow a composite *actor*, called after the ETS convergence loop, embedding a core-edge *actor*. Specifically, the multi-fluid edge plasma code SOLPS-B2 [24] has been coupled in

such a way to the ETS. The advantage of the implemented coupling is that any other 2D edge actor with the same inputs and outputs could replace the SOLPS actor directly.
In this approach, after each convergence loop of the ETS, SOLPS is called to update the boundary conditions for the core transport simulation. SOLPS takes as its inputs the fluxes of particles and energy from the *coreprof*, *coreimpur* and *coreneutrals* CPOs (Consistent Physical Objects [2]), uses these as its "core" boundary conditions, performs an iteration (which incorporates its own internal convergence loop), and returns updated values of the densities and temperature at the core-edge interface which are then used as the new "edge" boundary condition for the ETS core solution.
A challenge emerges on the physics side from the disparity on characteristic time-scales of the core and edge. For truly time-dependent calculations this problem is alleviated, though the accessible time-scales are limited by the maximum time-step that can be used in the edge code (for an ITER case without EIRENE, this is often 0.01 – 0.1 ms; with EIRENE the time-step might be limited to sub microseconds.). For steady state calculations, where the goal is to find core and edge solutions that are compatible, differential time-stepping is needed.

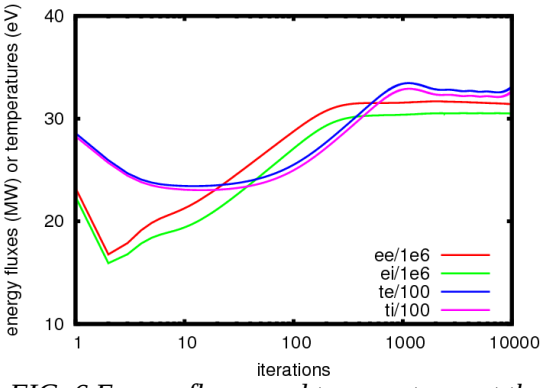

FIG. 6 Energy fluxes and temperatures at the core-edge boundary as a function of the number of iterations in the SOLPS loop.

In the coupled ETS-SOLPS case shown here as an example, D and T are simulated for an ITER case with the core-edge boundary 50 cm inside the outer mid-plane. In the ETS, Gaussian profiles are used to specify sources of particles and energy, and constant transport coefficients. The core time-step was 10ms, whereas the base time-step in SOLPS was 0.01ms, and the core part of the SOLPS simulation used a time-step of 1ms. Even with this choice, after 100s of core time, and 0.1s of SOL time (10000 iterations), slow changes are still present at the core-edge interface (FIG. 6), associated with a feedback loop in SOLPS which tries to bring the separatrix edge density to a desired value, emulating the sort of feedback loop that will be needed for target power control for ITER. The next step will be to include more species and physics in the core simulation.

4. MHD pedestal stability analysis of operational scenarios

An MHD linear stability analysis chain, pertinent to peeling-ballooning type instabilities has been released for the analysis of equilibria from any tokamak integrated in the EU-IM platform, including ITER and DEMO. The workflow includes the state-of-the-art high resolution equilibrium codes HELENA [25], CHEASE [19], CAXE [26] and linear MHD stability codes ILSA [27], MARS [28], MARS-F [29], KINX [26], implementing interoperability among all those whenever possible (e.g. KINX, capable of treating plasmas with a separatrix, requires a custom made grid provided by CAXE). The code pairs were cross-benchmarked within the workflow for core and global ideal kink instabilities, for JET and ASDEX-Upgrade equilibria [4]. The workflow can be plugged to equilibrium reconstruction [30] or a discharge simulator and used for interpretive studies on present devices.
Estimation of the MHD stability boundaries in operational plasma scenarios foreseen for future devices is also crucial. The predictive MHD *j*-α pedestal stability analysis workflow developed in the EU-IM framework - including at present HELENA and ILSA (with MISHKA1 kernel [31]) however easily replaceable by any of the above code pairs - has been applied to the analysis of the *EU DEMO1 2015* baseline scenario [18] sensitivity to plasma shape and core pressure as well as to assess JT-60SA scenarios stability.

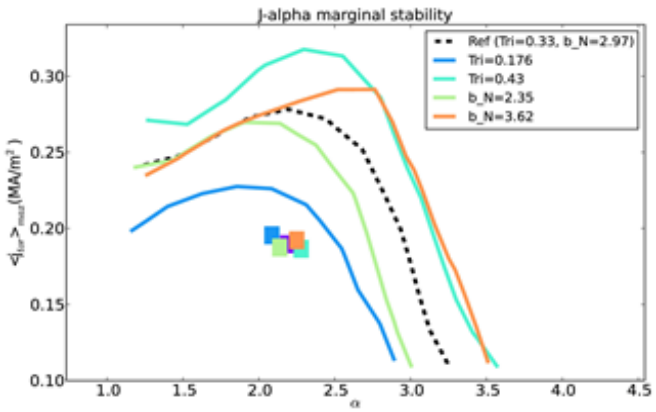

FIG. 7 Marginal stability curves (obtained at $\gamma\tau_A$~0.02 to account for diamagnetic stabilization contribution) for EU DEMO1 2015 scenarios (reference scenario in dashed line; operational points in squares), varying triangularity or core plasma beta (at constant pedestal profile and total current).

The DEMO1 sensitivity study addressed the effect of plasma triangularity and core plasma beta on the marginal stability against peeling, ballooning and peeling-ballooning instabilities.

A maximum toroidal mode number n=20 was used in all runs. The j-α analysis on the reference equilibrium shows that one is operating well into the stable region (FIG. 7 squares). Increases in triangularity/core beta shift the marginal stability curve (to a higher/lower extent) towards higher pressure gradients and edge currents (as it can be observed in FIG. 7), allowing for stable operation at increased pedestal pressure height/width.

The JT-60SA scenario stability assessment focused on currently established single-null scenarios [32], obtained imposing that the pedestal temperature follows the so-called Cordey two-term scaling [33]: the fully inductive Scenario 2 at low or high density and the hybrid Scenario 4, predicted with two different transport models. The two scenarios operate at substantially different pedestal pressure gradient and edge current (equilibria and profiles are summarized in FIG. 8), thus, although unstable to predominantly peeling-ballooning/ballooning modes, they stand quite differently with respect to the distance to the marginal stability boundary (as shown in FIG. 9). The different core plasma beta and triangularity (0.29 in Scenario 2 versus 0.42 in Scenario 4) concur to the different marginal stability curves.

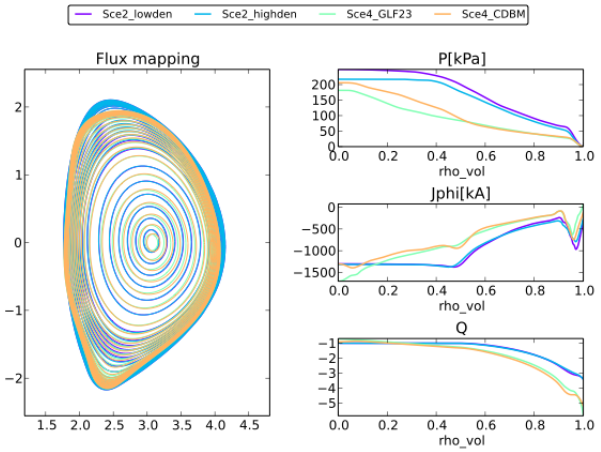

FIG. 8 JT-60SA magnetic equilibria produced by CHEASE, pressure, toroidal current and safety factor (Q) profiles for the four scenarios (all obtained with GLF23[34] transport model, whereas Scenario 4 was also run with CDBM[35]).

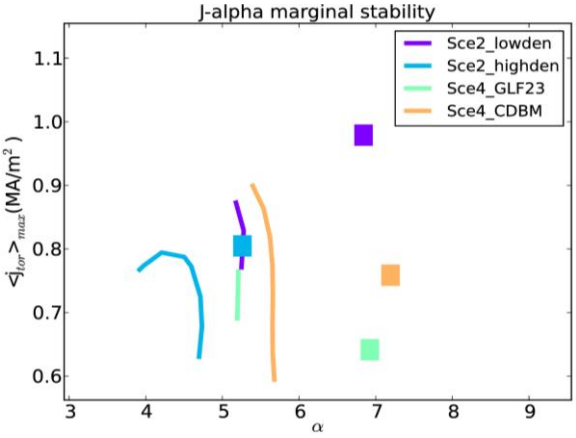

FIG. 9 Marginal stability curves (obtained at $\gamma\tau_A$~0.03 to account for diamagnetic stabilization) and operational conditions (colored squares) for the four JT-60SA scenarios of FIG. 8.

5. First-principle edge turbulence workflow

A turbulence workflow embedding the HESEL code [36] has been developed, which imports equilibrium parameters and diagnostic data from ASDEX-Upgrade database, and produces from the diagnostics implemented in HESEL, synthetic data for a Langmuir probe (at locations corresponding to the "*Stuttgart*" probe heads, as described in [37]) - and for Lithium

beam emission. The HESEL fluid model includes the transition from the confined region to the Scrape-Off-Layer (SOL) and the full development of the profiles across the Last Closed Flux Surface (LCFS) and is uniquely capable of reproducing essential features of L–H transitions. Electrically connected or disconnected divertor conditions are mimicked by applying different sheath boundary conditions - linking the electron potential to the electron temperature in the SOL [36].
The workflow has been applied to investigate the turbulent transport in the edge and SOL region at the outboard midplane of ASDEX Upgrade, in L-mode discharges, including detached ones, and is operational for the analysis of experimental data for SOL filamentary transport. Reasonable agreement has been observed between the synthetic probe data and the experimental measurements, comparing the momentum transport [37]. Furthermore, the energy flux, not accessible experimentally, has been investigated numerically [38,39].
An example of divertor power deposition is shown in FIG. 10 for a simulation using experimental parameters from ASDEX Upgrade, for a connected divertor case. Power depositions are mapped from the outboard midplane to the divertor surface using the magnetic field line geometry from AUG#30301. In HESEL the parallel dynamics for the electron and ion pressure equations in the SOL, is parameterized into an electron conductive part and an electron and ion advection part. The simulation results enlighten that in the near SOL the electron conductive part is dominant, whereas in the rest of the SOL the ion convective part is large and intermittent, as ion energy is transported radially outwards by blobs. The total power deposition at the divertor is split nearly equally between these two components, whereas the electron convective part is small.

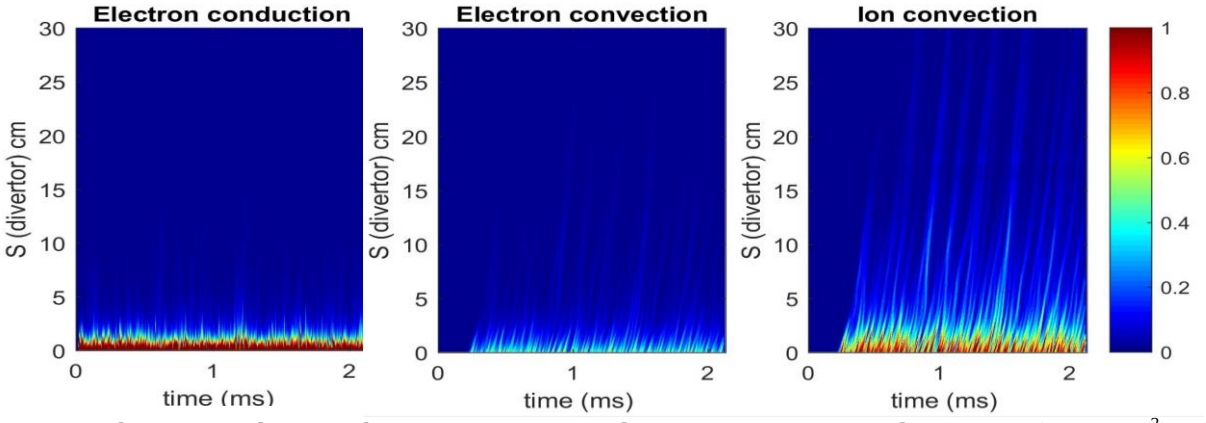

FIG 10 Electron conductive, electron convective and ion convective power depositions (in MW/m^2) on the divertor surface from an HESEL simulation using experimental ASDEX Upgrade parameters for a connected divertor case. The figures show the radial variations in a time span of 2.1msec (S is the coordinate along the divertor surface).

6. **Conclusions**

WPCD is developing complex modular workflows applicable to any tokamak including future devices such as JT-60SA, ITER and DEMO, within the standardized EU-IM framework, which offers the flexibility of interchanging and combining physics modules with different levels of accuracy in the physics description. In the future, IMAS [3, 40] will be adopted. Applications of the recently released fixed-boundary core European Transport Simulator, ETS and the j-α MHD pedestal stability workflow addressed predictions of reactor-like as well as JT-60SA scenarios. Further, the recent implementation in the ETS Kepler workflow of direct coupling of core and edge transport codes was demonstrated for the particular case of an ITER steady-state. Finally, application of an edge turbulence workflow to experimental ASDEX Upgrade probe data, allowed the interpretive analysis of SOL transport in connected divertor conditions, via direct comparison to synthetic diagnostics.

Acknowledgements This work has been carried out within the framework of the EUROfusion Consortium and has received funding from the Euratom research and training programme 2014-2018 under grant agreement No 633053. The views and opinions expressed herein do not necessarily reflect those of the European Commission.
The DEMO results here obtained using the EU-IM workflows are not meant as a basis on decision making on the design and parameters of the DEMO systems.

References

1. FALCHETTO, G.L. et al, Nucl. Fusion 54, 043018 (2014)
2. IMBEAUX, F. et al, Comp. Phys. Comm., 181(6), 987 – 998 (2010)
3. IMBEAUX, F. et al, Nuclear Fusion 55 (12), 123006, (2015)
4. COELHO, R. et al, 42nd EPS 2015 P4.178 ECA Vol. 39E ISBN 2-914771-98-3
5. BILATO, R. et al, 21st Topical Conference on Radiofrequency Power in Plasmas, 2015.
6. SCHNEIDER, M. et al, 42nd EPS 2015 P2.159 ECA Vol. 39E ISBN 2-914771-98-3
7. FOGACCIA, G. VLAD, G. AND BRIGUGLIO, S. Nucl. Fusion 56(11),112004 (2016)
8. KALUPIN, D. et al, Nucl. Fusion 53, 123007 (2013)
9. SCHNEIDER, M. et al, Nucl. Fusion 56 (11), 112022 (2016)
10. FIGUEIREDO, A.C.A. et al, 40th EPS 2013, P2.163 ECA vol.37D
11. ASUNTA, O. et al., 42nd EPS 2015 P2.156 ECA Vol. 39E ISBN 2-914771-98-3
12. ASUNTA, O. et al., Comp. Phys. Comm. 188, 33–46 (2015)
13. SCHNEIDER, M. et al, Nucl. Fusion 51, 063019 (2011)
14. HIRVIJOKI, E. et al., Comp. Phys. Comm. 185, 1310–1321 (2014)
15. WESSON, J., "Tokamaks", eq. (5.4.12) 3rd ed. 2004 (Oxford: Clarendon)
16. SCHNEIDER, M. et al, Nucl. Fusion 55, 013003 (2015)
17. SCHNEIDER, M.et al, Plasma Phys. Control. Fusion 47, 2087-2106 (2005)
18. WENNINGER, R. et al, 2016, Nucl. Fusion accepted for publication
19. LÜTJENS, H. et al., Comp. Phys. Comm. **97**, 219 (1996)
20. KALUPIN, D. et al, 42nd EPS 2015, P2.169 ECA Vol. 39E ISBN 2-914771-98-3
21. GAL, K. et al, Nucl. Fusion 48 085005 (2008)
22. KÖCHL, F. 35th EPS 2008 P4.099 ECA Vol.32D
23. Cross-sections from BOSCH AND HALE, Nucl. Fusion 32, 611 (1992)
24. SCHNEIDER, R. et al., Contrib. Plasma Phys. 46, 3 (2006)
25. HUYSMANS, G.T.A. et al., Computational Physics (Proc. CP90 Conf.), World Scientific Publishing Singapore (1991), p. 371
26. DEGTYAREV, L. et al., Comp. Phys. Comm. **103** (1997)
27. STRUMBERGER, E. et al., Nuclear Fusion 45, 1156 (2005)
28. BONDESON, A. et al., Phys. Fluids **B 4,** 1889 (1992)
29. LIU, Y. Q. et al., Phys. Plasmas **7,** 3681 (2000)
30. COELHO, R. et al., 43rd EPS 2016, P1.050, ECA Vol. 40A ISBN 2-914771-99-1
31. MIKHAILOVSKII, A. B. et al., Plasma Phys. Rep. 10, 844 (1997)
32. GARCIA, J. et al., Nucl. Fusion 54, 093010 (2014)
33. CORDEY, J.G. Nucl. Fus. 43, 670-674 (2003)
34. KINSEY, J.E. et al Phys. Plasmas 12, 052503 (2005)
35. HONDA, M. et al Nucl. Fusion 46, 580 (2006)
36. MADSEN, J. et al , Phys. Plasmas 23, 032306 (2016)
37. NIELSEN, A.H. et al, 42nd EPS 2015 P1.105 ECA Vol. 39E ISBN 2-914771-98-3
38. NIELSEN, A.H. et al, 43nd EPS 2016 P5.049 ECA Vol. 40A ISBN 2-914771-99-1
39. NIELSEN, A.H. et al, 2016, submitted to Plasma Phys. Control. Fusion
40. PINCHES S., et al., 26th IAEA Fusion Energy Conf. 2016, Kyoto, Japan, TH/P2-14